IOP Conf. Series: Materials Science and Engineering **430** (2018) 012032 doi:10.1088/1757-899X/430/1/012032

Exploring Micro-focus X-ray computed tomography for metal injection moulded green parts

M Seerane[1,2,3]

[1] Light Metals, Materials Science & Manufacturing, Council for Scientific and Industrial Research, Meiring Naudé Road, Brummeria, Pretoria 0185, South Africa
[2] Titanium Centre of Competence, Materials Science & Manufacturing, Council for Scientific and Industrial Research, Meiring Naudé Road, Brummeria, Pretoria 0185, South Africa
[3]School of Chemical and Metallurgical Engineering, University of the Witwatersrand, Johannesburg, South Africa

*mseerane@csir.co.za

Abstract: Metal injection moulding (MIM) involves mass production of simple to intricate near-net shape parts at a relatively low cost by blending metal powders of defined characteristics with a polymeric binder system. The blend, popularly known as a feedstock, is injected into a mould cavity of a desired shape to form a green part. Most defects such as cracks, sink marks and voids manifest during the injection stage of the process. Internal cracks and voids are impossible to visualise after injection moulding. Micro-focus X-ray computed tomography (μXCT) is one of the techniques that can be used to evaluate and characterise such defective features. μXCT is a non-destructive method that uses penetrating X-ray radiation to probe objects or samples and create a complete virtual 3D representation of the object to visualise the internal structures and morphologies such as porosity, voids, cracks and inclusions as well as their location and their distribution in 3D. This work is intended to explore the μXCT approach MIM green parts and characterise the internal defects. The samples were scanned at 135 keV and 100 μA for X-ray penetration and contrast while placed onto a rotating sample manipulator which facilitated scanning through 360°. The samples were then reconstructed and further analysed for volume (3D) graphics.

1. Introduction

Metal Injection Moulding (MIM) is a relatively new technology that produces near net shaped medium-to-complex metal components at low cost [1]. This process involves blending of a metallic powder with a polymeric binder to produce a feedstock for forming a part of desired shape. MIM consists of four basic steps: 1) blending 2) injection moulding 3) debinding 4) sintering [2]. Injection moulding forms part of the most critical steps in MIM and affects the subsequent steps in the process [3].

Defects such as weld lines, jetting, incomplete filling, air traps, gate and ejection pin marks are common during injection moulding. These defects are generated during mould filling and part ejection as a result of the process settings and the quality of the feedstock. It is, therefore, important that this step is fully understood and that the filling pattern of the feedstock into the mould cavity is well monitored. The process settings are studied and optimised in different ways. Some of the common methods of studying and obtaining the optimum process settings for injection moulding is Factorial

design and Taguchi approach [4], [5]. The filling pattern of the feedstock into the mould cavity and the evolution of defects is often difficult to trace and detect *in-situ*. Rheological models [6] and computer aided engineering (CAE) analysis [7] are normally adopted to predict the complex flow behaviour of the feedstock into the mould cavity.

For defect analysis, microscopic examination and visual inspection of the green parts have been useful methods to identify sample defects [8]. These examinations can be conducted destructively and non-destructively, respectively. Destructive inspection include breaking or slicing of the green part. Non-destruction examination includes penetrant inspection (PI), magnetic particle inspection (MPI) and eddy current testing (ECT). These inspections are chosen on the basis of the nature and size of the defect, or whether the defects are systematic or random. Defects can be located either on the surface of the green specimen or internally. Surface defects are easily identified and can be located visually or through PI, MPI and ECT. However, internal defects are more difficult to detect using the latter traditional techniques unless the suspected internal defect generates an external morphology. In addition, MPI is only limited to ferromagnetic materials such as Fe, Ni, Co and their alloys; whereas ECT requires conductive materials and PI is suitable for materials with relatively non-porous surface. Scanning electron microscope (SEM) and optical microscope (OM) are suitable tools for analysing defects from sintered components; also, these techniques are limited to surface analysis.

It is therefore important to adopt methods that can resolve and characterise internal porosity and defects (large or small) of a sample. Large internal defects can be detected using radiography or ultrasonic echography. The biggest challenge is encountered when the defects are less than 1 mm in dimension. Micro-focus X-ray computed tomography (μXCT) is becoming an attractive technique to resolve and characterise defects as small as 1 mm. μXCT is a non-destructive radiation based technique for high quality micron-level information of the interior as well as composition of samples [9]. This technique uses an X-ray beam to probe objects or samples to create a complete virtual 3D volume that reveals internal structures such as defects, porosity and inclusions at high spatial resolution better than 1 μm [10], [11]. However, the big limitation in to this system is that the focal spot is relatively large (3 mm) and as a result the spatial resolution obtained, even with small sample, is in the order of 0.08 mm. Also, metals are often a challenge due to the relatively higher absorption of the X-rays. This is normally improved by increasing the X-ray energy. The technique is commonly applied in geoscience, archaeological science and medical field.

μXCT is gaining a lot of attention in MIM for quality inspection and process optimisation. Muchavi et al. [12] adopted this technique to explore and characterise the size, concentration and distribution of pores in MIM green and sintered parts. It was claimed that the technique can be used as a reliable tool to reveal detailed 3D internal structure of MIM parts qualitatively and quantitatively. Mannschatz et al. [13] and Yang et al. [14] used this method to analyse MIM parts and optimise the process. However, the authors did not give a detailed information on how the technique works. Hoffman and De Beer [9] and Bam et al. [10] outlined the characteristics of μXCT facility at Necsa and how it can be applied in geological science. This work is aimed at exploring and understanding the capabilities of μXCT technique in MIM research, especially for MIM practitioners who are beginning to adopt the technique.

2. Materials and experimental approach

The MIM green components were produced from titanium alloy powder and wax-based binder using a 40 tonne ARBURG Allrounder 400-70 injection moulding machine. Injection moulding trials were done through design of experiments (DoE) approach and each trial process parameters were recorded. The injection moulding parameters used are shown in Table 1. A total number of trials for each combination of the parameter values was reduced to 9 using Minitab software as a DoE tool. The specimens made are tensile test specimens with dimensions 89 mm (overall length), 40 mm (gauge length), 14.8 mm (grip section diameter) and 5 mm (gauge section diameter) (See figure 1).

Table 1. Injection moulding parameters

	Factor	Level		
		1	**2**	**3**
A	Injection temperature [°C]	130	135	140
B	Injection pressure [Bar]	600	700	800
C	Volumetric Injection speed [$cm^3.s^{-1}$]	30	40	50
D	Mould temperature [°C]	30	40	50

The samples were taken for tomography scans. The scanning unit is a Nikon XTH 225L µXCT (Nikon Metrology, Leuven, Belgium) based at the MIXRAD laboratory at the South African Nuclear Energy Corporation (NECSA, Pelindanba). Important scanning parameters include X-ray energy, exposure time, beam current and number of projections. A combination of these parameters give different image contrasts and quality for optimal data acquisition. The MIM specimens were mounted on a polystyrene mould and placed onto a 360° rotating sample manipulator for scanning process. After scanning, the samples were then reconstructed using Nikon CTPro software (Nikon Metrology, Leuven, Belgium) to transform 2D projections into virtual 3D volumes. The reconstruction parameters are optimised automatically for quality scanning to avoid error of measurements by the operator. The samples were further analysed using VGStudioMax V2.2 (Volume Graphics GmbH, Heidelberg, Germany) for material-volume isolation and defect/pore/inclusion identification.

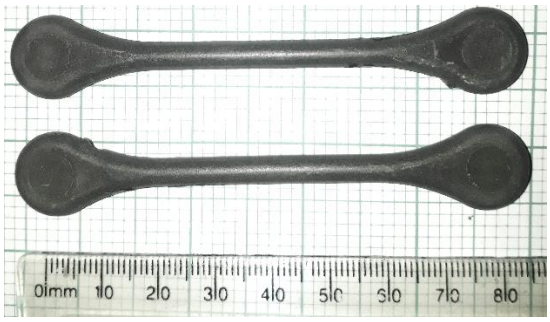

Figure 1. MIM green parts as tensile test specimens

Figure 2 shows a micro-focus XCT process from beam release to part reconstruction and analysis. An X-ray beam is released from the source to interact with the sample. A filter, normally copper, is placed in front of the specimen to remove low/weak energy X-rays to avoid beam hardening. Another common artefact is cone beam artefact which result from the positioning of the specimen within the beam. High energy X-rays interact with the sample and are attenuated. The attenuated beam is collected by the detector. The detector projections are reconstructed within a field of view at a full rotation of 360°. This stage allows optimum image acquisition and the reduction of artefacts such as misalignment artefacts, ring artefacts and line artefacts [10]. The acquired image is transformed from 2D (pixels) to 3D (voxels) volume. This volume is then analysed for internal features.

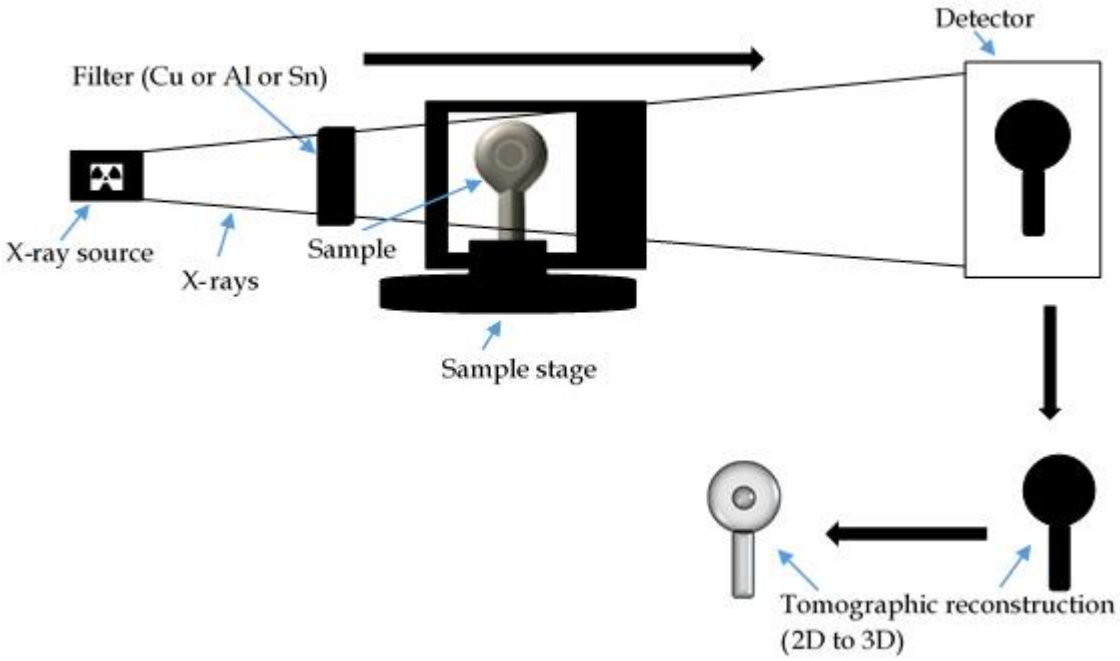

Figure 2. A schematic representation μXCT process

3. Results and discussion

Figure 3(a-d) shows a sequential process of the reconstructed MIM test piece from material isolation to a 3D volume using a VGStudioMax. In Figure 3(b) the volume is isolated from the material to reveal the surface and internal features of the sample. Blisters and bubble-like defects can be seen. Further analysis show finely distributed pores and cracks on the sample volume (Fig. 3c and d). These defects resulted from a set of conditions as follows: injection temperature – 140 °C, injection pressure – 800 bar, injection speed – 40 $cm^3.s^{-1}$ and mould temperature – 30 °C. The order of these defects and pores were quantified in the range of 0.01 to 2.03% combined, using VGStudioMax. This type of defects affect MIM subsequent processes such as debinding and sintering since they act as crack initiation sites and weak areas during mechanical testing, and hence part failure. This technique has proved to be a reliable source to reveal and quantify surface and internal features of MIM samples without any destruction, whereas other NDT test methods (ECT, MPI and PI) can only analyse surface defects and that the defects cannot be easily quantified.

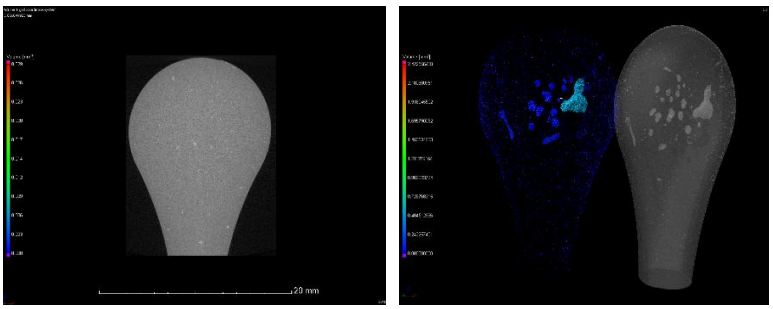

a) b)

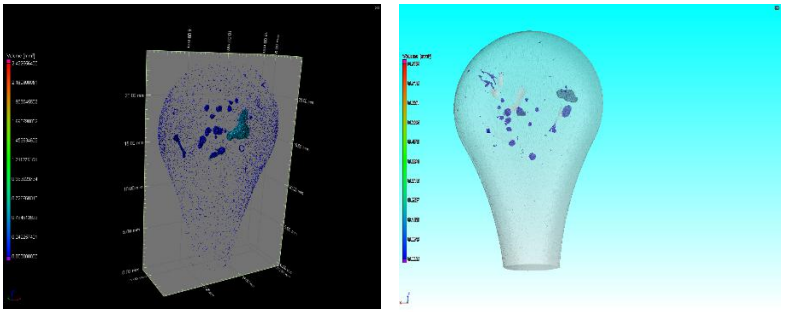

c) d)

Figure 3. Transformation of the acquired sample from pixels (2D) to voxels (3D): (a) reconstructed 2D image, (b) voxel isolation (c) voxel analysis (d) completed 3D volume

Figure 4 shows a 3D volume of MIM sample produced from optimum MIM process and it can be clearly seen that the sample does not contain any defects, both internally and externally. The defect free optimum process parameters are as follows: injection temperature – 130 °C, injection pressure – 800 bar, injection speed – 40 $cm^3.s^{-1}$ and mould temperature – 40 °C. The porosity level was found to be 0.01% and this is acceptable for MIM green parts.

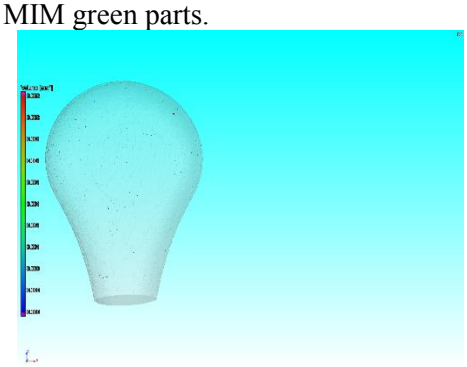

Figure 4. A test piece volume produced from MIM optimised process parameters

4. Conclusions

The µXCT technique was explored using MIM test piece samples produced at the CSIR. The technique proved to be a quick, reliable and most effective source to analyse not only geoscience, medical and archaeological samples but also MIM samples with no significant limitation in terms of material type and sample size. Also, the technique was able to reveal internal features of the part unlike traditional NDT methods such as ECT, MPI and PI. Set of parameters that led to noticeable defects during injection moulding were found to be as follows: injection temperature – 140 °C, injection pressure – 800 bar, injection speed – 40 $cm^3.s^{-1}$ and mould temperature – 30 °C. However, the optimum set of parameters that showed no signs of defects were 130 °C for injection temperature, 800 bar for injection pressure, 40 $cm^3.s^{-1}$ for injection speed and 40 °C for mould temperature.

Acknowledgements

The author would like acknowledge the Council of Science and Industrial Research (CSIR) and Department of Science and Technology (DST) for funding this work. The author also extends acknowledgements to the South African Nuclear Energy Corporation (NECSA), MIXRAD laboratory for providing a µXCT facility and lessons, in particular Mr. L. Bam and Mr. FC De Beer.

References

[1] Li S, Huang B, Li Y, Qu X, Liu S and Fan J 2003 *J. Mater. Process. Techno.* **137** 70–73.
[2] Moballegh L, Morshedian J and Esfandeh M 2005 *Mater. Lett.* **59** 2832–2837.
[3] Fang W, He X, Zhang R, Yang S and Qu X 2014 *Powder Technol.* **256** 367–376.

[4] Kamaruddin S, Khan Z A and Foong S H 2010 *Int. J. Eng. Technol.* **2**
[5] Packianather M, Chan F, Griffiths C, Dimov S and Pham D T 2013 *Procedia CIRP* 12 300–5.
[6] Machaka R, Ndlangamandla P and Seerane M 2018 *Powder Technol.* 326 37–43.
[7] Shin K, Heo Y, Park H, Chang S and Rhee B 2013 *Materials (Basel)* 6 5878–92.
[8] Schlieper G, Dowson G and Williams B 2013 *Metal injection moulding*, 3rd ed. Shrewsbury (European Powder Metallurgy Association).
[9] Hoffman J W and de Beer F C 2012 *18th World Conf. Nondestruct. Test.* 1–12.
[10] Bam L C, Miller J A, Becker M, de Beer F C and Basson I 2016 *The Third Ausimm International Geometallurgy Conference* 15–6.
[11] Landis E N and Keane D T 2010 *Mater. Charact.* **61** 1305–16.
[12] Muchavi N S, Bam L, de Beer F C, Chikosha S and Machaka R 2016 *J. South. African Inst. Min. Metall.* **116** 973–80.
[13] Mannschatz A, Müller A and Moritz T 2011 *J. Eur. Ceram. Soc.* **31** 2551–2558.
[14] Yang S, Zhang R and Qu X 2015 *Mater. Charact.* **104** 107–115.